Published in final edited form as:
Nat Microbiol. 2018 July ; 3(7): 814–823. doi:10.1038/s41564-018-0177-8.

Modeling *Cryptosporidium* infection in human small intestinal and lung organoids

Inha Heo[#1], **Devanjali Dutta**[#1], **Deborah A. Schaefer**[2], **Nino Iakobachvili**[3], **Benedetta Artegiani**[1], **Norman Sachs**[1], **Kim E. Boonekamp**[1], **Gregory Bowden**[4], **Antoni P.A. Hendrickx**[5], **Robert J.R. Willems**[5], **Peter J. Peters**[3], **Michael W. Riggs**[2], **Roberta O'Connor**[4,§], and **Hans Clevers**[1,6,§]

[1]Hubrecht Institute, Oncode Institute, Royal Netherlands Academy of Arts and Sciences (KNAW), Uppsalalaan 8, 3584 CT, UMC Utrecht, 3584 GC, Utrecht, the Netherlands [2]School of Animal and Comparative Biomedical Sciences, College of Agriculture and Life Sciences, University of Arizona, Tucson, AZ 85721, USA [3]The Maastricht Multimodal Molecular Imaging Institute (M4I), Universiteitssingel 50, Maastricht 6229 ER, The Netherlands [4]Veterinary Microbiology and Pathology, College of Veterinary Medicine, Washington State University, Pullman, WA. 99163, USA [5]Department of Medical Microbiology, University Medical Center Utrecht, Heidelberglaan 100, 3584 CX Utrecht, the Netherlands [6]Princess Máxima Centre, 3584 CT, Utrecht, the Netherlands

[#] These authors contributed equally to this work.

Abstract

Stem cell-derived organoids recapitulate *in vivo* physiology of their original tissues, representing valuable systems to model medical disorders such as infectious diseases. *Cryptosporidium*, a protozoan parasite, is a leading cause of diarrhea and a major cause of child mortality worldwide. Drug development requires detailed knowledge of the pathophysiology of *Cryptosporidium,* but experimental approaches have been hindered by the lack of an optimal *in vitro* culture system. Here we show that *Cryptosporidium* can infect epithelial organoids derived from human small intestine and lung. The parasite propagates within the organoids and completes its complex life cycle. Temporal analysis of the *Cryptosporidium* transcriptome during organoid infection reveals

[§]Authors for correspondence: rob.oconnor@wsu.edu; h.clevers@hubrecht.eu.

Conflict of interest
N.S. and H.C. are inventors on patents/patent applications related to organoid technology.

Data availability
RNA sequencing data that support the findings of this study have been deposited in Gene Expression Omnibus (https://www.ncbi.nlm.nih.gov/geo) with the accession code (GSE112991)

Author contributions
I.H. designed, performed and analyzed the experiments, and wrote the manuscript. D.D. designed, performed the experiments, and helped analyzing data. D.S. and M.R. performed mice experiments. N.I. and P.P. performed TEM experiments. B.A. helped performing RNA sequencing and analyzing the data. N.S. helped the experiments with lung organoids and immunofluorescence microscopy imaging. K.B helped the qPCR experiments. R.O. performed oocyst isolation from organoids. G.B. and R.O. performed GO-term analysis of *C. parvum* genes. A.H. and R.W. helped SEM experiments. R.O. and M.R. analyzed SEM and TEM data. H.C. and R.O. supervised the project and H.C. wrote the manuscript. All the authors commented on the manuscript.

Europe PMC Funders Author Manuscripts

dynamic regulation of transcripts related to its life cycle. Our study presents organoids as a physiologically relevant *in vitro* model system to study *Cryptosporidium* infection.

Introduction

In a culture medium mimicking *in vivo* niche conditions, adult epithelial stem cells can be grown into 3D organoids that recreate crucial aspects of the architecture, the cellular make-up and the function of the original epithelium1. Adult stem cell-derived organoids contain most differentiated cells present in the tissue of origin and can expand long-term without exhibiting significant genomic instability1. Of note, human small intestinal (SI) organoids can be grown under two different culture conditions. In a Wnt-rich culture medium, organoids comprise mainly of stem cells and their highly proliferating progenitor cells ('expanding organoids'). Upon withdrawal of Wnt, the expanding organoids differentiate to form enterocytes, goblet cells, and enteroendocrine cells ('differentiated organoids')2.

Cryptosporidium is an apicomplexan parasite causing a diarrheal disease called cryptosporidiosis3–5. As an obligate parasite, *Cryptosporidium* completes its life cycle only within a suitable host. Infection begins with the ingestion of sporulated oocysts by the host (Fig. 1a). In the SI lumen, oocysts undergo excystation and release four sporozoites. The sporozoites invade the apical surface of epithelial cells and develop into trophozoites within parasitophorous vacuole, a closed epicellular compartment made of host and parasite-derived membrane4. The trophozoites undergo asexual replication and develop into six to eight merozoites (meront I). The merozoites are released and reinvade adjacent cells to form additional meronts I or meronts II. A meront II releases four merozoites that enter host cells to form sexual stages: the microgamont (male form) or the macrogamont (female form). During fertilization, a microgamete is released from a microgamont and fuses with a macrogamont to form a zygote that develops into a new oocyst. The newly formed oocysts are released into the lumen and excreted with feces from the host.

While *Cryptosporidium* infection induces self-limiting diarrhea and is often asymptomatic in immunocompetent individuals, it results in life-threatening severe diarrhea in immunodeficient hosts such as AIDS patients, malnourished children and elderly people6–8. While the intestine is the primary infection site of *Cryptosporidium*, the respiratory tract can also be targeted, causing respiratory cryptosporidiosis in both immune-competent and -deficient individuals9, 10. Recently, the Global Enteric Multicenter Study (GEMS) reported that *Cryptosporidium* is a major cause of morbidity and mortality in infants in developing countries11. Despite the global importance of this disease, there is no vaccine available. There is a single FDA-approved drug (Nitazoxanide) that is not effective in immunodeficient patients12, 13. A main challenge to *Cryptosporidium* study and drug development has been the establishment of optimal *in vitro* culture systems to recapitulate *in vivo* infection. Molecular mechanisms of the pathophysiology of the parasite thus remain largely unidentified14, 15.

Several *in vitro* culture systems have been reported to model *Cryptosporidium* infection16, 17. Two dimensional (2D) cultures of colorectal adenocarcinoma cell-lines have been most frequently used, while examples of mono-layered cultures of primary cells have also been

Europe PMC Funders Author Manuscripts

Europe PMC Funders Author Manuscripts

reported16, 18, 19. However, most of these only support short-term infection (< 5 days) and support incomplete propagation of the parasites. Recent studies using bioengineered 3D cultures of colorectal cancer cell lines resulted in more efficient and longer infection of the parasites20, 21. Yet, transformed cancer cell lines –rather than primary cells- were used in these studies, which cannot fully recapitulate *in vivo* host-parasite interaction.

Organoids have been exploited to model diseases including cancer, hereditary diseases, as well as viral and bacterial diseases22–24. Here we infect intestinal and lung organoids derived from healthy human donors with *Cryptosporidium*. We find that *Cryptosporidium* can replicate within the organoids and complete its entire life cycle. Our study shows that human organoids represent physiologically relevant *in vitro* model systems for *Cryptosporidium* infection.

Results

Human intestinal organoids support asexual and sexual stages of *C. parvum* life cycle

To investigate whether human SI organoids can be used as an *in vitro* culture system for *Cryptosporidium*, we infected expanding and differentiated SI organoids with *Cryptosporidium parvum* (*C. parvum*; one of the most common *Cryptosporidium* species responsible for infection in humans). Because the apical side of the epithelial cells faces the lumen of the organoids, we introduced oocysts into the lumen of the organoids by microinjection (Fig. 1b). To examine whether the parasites could propagate within the organoids, we quantified the presence of parasites at different time points after injection by qPCR of *C. parvum* 18S rRNA (Fig. 1c). In both expanding and differentiated organoids, *C. parvum* rRNA increased by orders of magnitudes at 1 day post-infection. Parasite presence remained high at day 6. Of note, *C. parvum* infection and propagation was about 10 fold more efficient in differentiated organoids than in expanding organoids, suggesting that *C. parvum* mainly targets differentiated cells.

To address whether *C. parvum* can cycle through its developmental stages within organoids, we first performed scanning electron microscopy (SEM) imaging. We observed injected oocysts inside organoids directly after injection (Supplementary Fig. 1a). After 6 hr, we captured the moment when sporozoites excysted from the oocysts and observed early trophozoites near empty oocysts (arrow and arrowhead in Supplementary Fig. 1b, respectively), indicating that sporozoites invaded epithelial cells in organoids and developed into the next stage. Other epicellular structures including meronts I and II formed over time (arrow and arrowhead in Supplementary Fig. 1c, respectively). In addition, abnormally elongated microvilli around trophozoites and meronts were occasionally observed, which was previously reported in the SI of *C. parvum* infected mice (arrow in Supplementary Fig. 1d)25. Together, these results suggested that *C. parvum* could propagate within organoids and that the phenotype observed *in vivo* could be recapitulated in organoids.

To clarify the identity of the epicellular stages within organoids, we performed immunofluorescence assays (IFA) using an antibody (Sporo-Glo) that detects *C. parvum* stages. Because each stage harbors a different number of ‘zoites’ (such as sporozoites, merozoites, and microgametes in Fig. 1a) and thus a distinct number of nuclei, dual staining

with Sporo-Glo and DAPI allowed determination of individual stages. We observed meronts I and possibly meronts II with 8 and 4 nuclei, respectively, at 24 hr after injection, and detected microgamonts carrying 16 nuclei at 72 hrs in organoids (Fig. 1d). To further ascertain the progression of the parasite life cycle, we performed transmission electron microscopy (TEM) imaging. We observed most epicellular stages including invading sporozoite, trophozoite, releasing merozoites, empty parasitophorous vacuole, meront II, macrogamont, zygote, and developing oocyst in organoids at various time points after injection (Fig. 1e and Supplementary Fig. 1e)26–28. Altogether, our results implied that *C. parvum* could develop most stages efficiently within organoids. In addition, TEM images of differentiated organoids showed that the parasite infected maturing enterocytes (Supplementary Fig. 1f).

C. parvum can complete the entire life cycle within intestinal organoids

Next, we investigated whether the parasites could complete their full life cycle by generating new oocysts within SI organoids. To exclude the possibility that injected oocysts obscured the detection of newly formed oocysts, we isolated sporozoites after *in vitro* excystation and microinjected them into organoids (Fig. 2a). Like oocysts, sporozoites developed epicellular stages including trophozoites and meronts within organoids (Supplementary Fig. 2a and b). IFA showed that oocysts (oocyst-specific Crypt-a Glo) were detected within organoids at 72 hrs after injection, while only sporozoite signals (anti-gp15 antibody) were observed at 1 hr (Supplementary Fig. 2b), indicating that oocysts were generated from the sporozoites. Furthermore, to examine that the oocysts were released into the lumen of the organoids as in the *in vivo* situation, we mechanically dissociated the infected organoids and isolated oocysts from the organoid lumen by using oocyst-specific antibody-conjugated magnetic beads. IFA using Crypt-a-Glo clearly showed isolated oocysts which were confirmed by TEM imaging (Fig. 2b and Supplementary Fig 2c). Together, these data indicate *C. parvum* can undergo its full replicative cycle in organoids, including the apical shedding of newly produced oocysts.

We further determined whether the newly formed oocysts were infectious. At 4 day post-injection, we mechanically dissociated sporozoite-injected organoids and introduced these into neonate mice through oral gavage (Fig. 2d)29, 30. One week after inoculation, we examined the degree of infection in the mice intestine by qPCR of the parasite heat shock protein 70 gene (HSP70) (See Methods)31. Mice inoculated with injected organoids showed levels of infection comparable to mice infected with oocysts obtained from calves while mice treated with control organoids did not display any infection (Supplementary Fig. 2c). Although we previously reported that sporozoites were vulnerable to stomach passage through oral inoculation32, the infectivity of the other stages has not been studied. To exclude the possibility that other epicellular stages of the parasite inside organoids might infect the mice, we inoculated sporozoite-injected organoids into mice at 1 day post-injection (S_1d) and compared these with the mice inoculated with sporozoite-infected organoid for 5 days (S_5d) (Fig 2c). Sporozoites developed different stages such as trophozoites, meront I and II but did not form oocysts within 1 day after injection (Fig 1d, e and Supplementary Fig 2e). While the mice inoculated with S_5d organoids induced significant infection by the parasite, introduction of S_1d organoids did not display any

infection in the mice, indicating that infectious particles are not yet present at 1 day (Fig 2c, one-way ANOVA analysis, *p*-value=0.011). Histological sections of the intestine from the mice confirmed that only the mice inoculated with S_5d organoids showed parasite infection in the ileum-cecum junction, a main targeting site of the parasite infection within intestine (Fig. 2d). Together, the mouse experiment shows that human intestinal organoids support the completion of the parasite's entire life cycle from sporozoites to infectious oocysts.

To probe the potential of long-term culturing of the parasite within organoids, we injected sporozoites into expanding organoids and examined the maintenance of the parasite infection in organoids after passaging. To increase the efficiency of infection and propagation of the parasite, we induced differentiation of the organoids shortly after injection and switched back to the expansion condition 1 day before splitting (See Methods). Through this switching between expansion and differentiation conditions, the parasites persisted within organoids for at least 28 days, or 3 passages of organoid culture (Supplementary Fig. 3). We did note a gradual decline after passaging.

Human lung organoids model *C. parvum* infection

While infection of *C. parvum* in respiratory tract has been reported previously, the pathophysiology of respiratory infection remains largely unknown9, 10. Thus, we sought to use human lung organoids to model respiratory infection of the parasite. We have recently established human airway epithelial organoid which recapitulates bronchial airway. Lung organoid consists of basal cells, ciliated cell, goblet cells and club cells33. To examine whether the parasite can infect lung organoid and complete the life cycle, we microinjected oocysts into organoids and collected the organoids at various time points for qRT-PCR and IFA. Quantification of 18S rRNA showed that parasite increased dramatically within 24 hrs after injection, similar to the parasite growth within SI organoids in Fig. 1c (Fig. 3a). By performing IFA using zoite-specific antibody, we verified the development of asexual (meront I) and sexual (microgamont) stages within organoids (Fig. 3b). From TEM imaging, we also observed that the parasite could infect secretory cell as well as non-secretory cells in lung organoid (Supplementary Fig. 4). Lastly, IFA of sporozoite-infected organoids using Crypt-a-Glo showed newly formed oocysts at 6 day post-infection (Fig. 3c). Taken together, we concluded that human lung organoids allow the propagation of *C. parvum* and the completion of the full life cycle of the parasites.

Transcriptome analysis of host epithelial cells and *C. parvum*

We next performed high-throughput RNA sequencing using differentiated SI and lung organoids at 24 and 72 hr post-infection. Media-injected organoids were used as a control. Gene expression changes were already observed at 24 hr (red dots, *p*-value < 0.05 in Fig. 4a) and the number of differentially expressed genes upon infection increased after 72 hrs in both SI and lung organoids (Fig. 4a and Supplementary Table 1). GO (gene ontology)-term analysis revealed that a substantial number of genes related to 'cytoskeleton' and 'cell mobility' were up-regulated in lung organoids at 24 hr post-injection, suggesting that parasite infection and subsequent formation of epicellular stages might affects cytoskeleton structures of host cells (Fig. 4b). After 72 hrs, many genes associated with the type I interferon pathway increased dramatically in lung organoids (top in Fig. 4c), which was

confirmed using Gene Set Enrichment Analysis (GSEA) with significance score (bottom in Fig. 4c, nominal *p*-value < 0.01). Although the number of differentially expressed genes in SI organoids was lower than that in lung organoids, the genes related to the type I interferon pathway were also enriched upon infection (Supplementary Fig. 5 and Table 1). While type II interferon has long been considered an important immune factor in response to parasite infection, type I interferon has recently emerged as an anti-parasite effector34, 35. Our results support that type I interferon signaling is induced in epithelial cells as a response to infection by *C. parvum*.

Next, we analyzed changes in expression in the transcriptome of *C. parvum* from the same sequencing data sets. Multiple *C. parvum* genes were differentially expressed with a large fold change between 24 and 72 hr post-injection (Magenta dot, *p*-value < 0.05 in Fig. 4d). GO analysis of the differentially expressed genes revealed substantial differences of protein functions between 24 and 72 hr in both SI and lung organoids, indicating that distinct developmental stages of the parasites formed at these two time points (Supplementary Fig. 5 and Table 2). At 24 hr, most of the enriched genes represented ribosomal proteins and ribosomal RNA subunits, suggesting that intensive biomass production occurred (Fig. 4e and Supplementary Fig. 5, 6). It is consistent with the results in Fig. 1c and 3a that the parasites proliferated massively within 24 hrs. By contrast, at 72 hr, multiple oocyst-wall protein genes were up-regulated, confirming that the parasites formed oocysts (Fig. 4e and Supplementary Fig. 6). Taken together, these data illustrate molecular events occurring in both host cells and the parasite during infection and propagation of the parasite.

Discussion

In this study, we evaluate the usefulness of human intestinal and lung organoids as an *in vitro* culture system for *C. parvum.* We show that the parasite propagates and completes its complex life cycle within organoids. Newly generated oocysts from organoids are infectious and appear equivalent to oocysts obtained from an infected host animal.

To reveal a potential cell type dependency of parasite infection, we exploited a feature of human intestinal organoids i.e that organoids can be cultured under conditions that favor progenitor cells and that favor the generation of differentiated cells. Injection of the parasites into the two types of organoids demonstrated that *C. parvum* infected and propagated more efficiently in differentiated organoids than in highly proliferating expanding organoid. Our TEM imaging of differentiated SI organoids showed that enterocytes are mainly infected by the parasite, consistent with a previous report5. Despite a lower efficiency of the infection, expanding organoids do support the completion of the full life cycle of the parasites. As the host cytoskeleton is reported to be important for *C. parvum* invasion and establishment of epicellular stages, we suspect that rapid division of expanding organoids might inhibit the development of infection and subsequently reduce propagation of the parasite36, 37. It is also possible that specific receptors for *C. parvum* infection might be mainly expressed in differentiated cells. Further studies need to clarify the mechanisms of cell type specificity of infection.

C. parvum has been reported to infect the respiratory tract to result in respiratory cryptosporidiosis9. Our organoid culture system derived from human healthy bronchial airway demonstrates, for the first time, the infection and propagation of *C. parvum* in lung epithelia *in vitro.* As observed in SI organoids, *C. parvum* establishes various epicellular stages and forms oocysts within lung organoids. This implies that lung organoids replicate the *in vivo* conditions of infection and thus can be used as a valuable tool to study tissue specific pathophysiology of the parasite.

RNA sequencing revealed host epithelial responses upon parasite infection in both differentiated SI and lung organoids. More host genes were regulated in lung organoids compared to SI organoids (Fig. 4a). It is possible that a higher percentage of cells was infected within an individual lung organoid because the general size of lung organoids is much smaller than that of SI organoids (by 5-8 fold). Yet, we cannot exclude the possibility that cells in lung might be more sensitive to parasite infection than intestinal cells. Despite the different efficiencies, we observed upregulation of genes associated with type I interferon immunity in both SI and lung organoids. While type II interferon has been well studied for anti-parasite immunity, the role of type I interferon in anti-parasite response remains incompletely understood34. While it has been reported that type I interferon partially inhibits the infection of *C. parvum* in 2D cancer cell-lines, type I interferon can also enhance bacterial infection by suppressing type II interferon that mainly protects host cells from parasites in animal models35, 38, 39. It will be of great interest to understand the physiological roles of type I interferon in *C. parvum* infection.

Recently, Aldeyarbi et al. reported that *C. parvum* could complete its life cycle in cell-free culture conditions within a few days. Using this system, the authors provided high-resolution TEM images of each epicellular stage26–28. This axenic system however does not recapitulate the interaction of host epithelia and the parasite. RePass et al. established a 3D culture system by employing a silk scaffold seeded with colon cancer cell lines Caco2 and HT29-MTX21. This system supports continuous culture for 17 days and production of oocysts. The authors however did not show that new oocysts were functionally comparable to normal oocysts in *in vivo* infection. Likewise, Morada et al. developed a 3D culture system by providing polysulphone hollow fibers seeded with colon cancer cell line, HCT-8[202020]. This system supports continuous culture for 6 months and *in vitro* production of oocysts which are infectious to mice. However, the hollow fiber system is not amenable for investigation of individual stages of the parasite life cycle and the interaction between host cells and the parasites. Both these systems employ transformed tumor cell lines rather than native healthy host cells. In contrast, organoids derived from healthy human tissues replicate the functional cell composition and 3D structure of original tissues1. They provide a physiologically relevant system for parasite infection in both intestinal and lung tissues. In addition, because organoids can be adjusted to 2D cell cultures40, it is easily adaptable for various experimental uses – from investigating parasite development and interactions with host cells to screening drugs. Additionally, because organoids contain purely epithelial cells, it allows studying direct interaction between host epithelia and the parasite. However, the current organoids system can still be improved. Although organoids can support continuous culture of the parasites for 28 days, parasite numbers decreased over time. Also, the number of oocysts formed within organoids was smaller than in host animals. For more complex

Europe PMC Funders Author Manuscripts

interactions with the host, establishment of organoid- immune cell co-cultures, will be required. Furthermore, genetic manipulation of *Cryptosporidium* has been recently reported41. Generation of genetically modified parasites in combination with an organoid culture system would allow more rapid dissection of the functions of specific parasite proteins in host-parasite interactions.

Methods

Human tissue materials

Small intestinal (SI) organoids were established from duodenal biopsies from healthy human donors in the previous work42. Endoscopic duodenal biopsy samples were obtained from individuals of different ages that had been admitted for suspected inflammation. The individuals were found to be healthy based on standard histological examination. Endoscopic biopsies were performed at the University Medical Center Utrecht and the Wilhelmina Children's Hospital. The patients' informed consent was obtained, and this study was approved by the ethical committee of University Medical Center Utrecht.

Lung organoids were established from normal region of bronchial airway tissue resection from non-small-cell lung cancer patients33. The collection of patient data and tissue for the generation and distribution of organoids has been performed according to the guidelines of the European Network of Research Ethics Committees (EUREC) following European, national, and local law. In the Netherlands, the responsible accredited ethical committees reviewed and approved the studies in accordance with the 'Wet medisch-wetenschappelijk onderzoek met mensen' (medical research involving human subjects act). The 'Verenigde Commissies Mensgebonden Onderzoek' of the St. Antonius Hospital Nieuwegein approved protocol Z-12.55. All patients participating in this study signed informed consent forms approved by the responsible authority. In all cases, patients can withdraw their consent at any time, leading to the prompt disposal of their tissue and any derived material. Lung organoids established under protocols Z-12.55 were biobanked through Hubrecht Organoid Technology (HUB, www.hub4organoids.nl). Future distribution of organoids to any third (academic or commercial) party will have to be authorized by the METC UMCU at request of the HUB in order to ensure compliance with the Dutch medical research involving human subjects' act.

Organoid culture

Small intestinal (SI) organoids were established from duodenal biopsies from healthy human donors in the previous work42. Briefly, dissociated SI crypts were isolated from biopsy and embedded in Matrigel (BD Biosciences), and were overlaid with a Wnt-rich medium (for expanding organoid) containing Advanced DMEM/F12 with 1x Glutamax, 10mM HEPES, penicillin-streptomycin, 1x B27 (all from Invitrogen), 1μM *N*-Acetylcysteine (Sigma), 20% R-spondin1 conditioned medium, 10% Noggin conditioned medium, 50ng ml^{-1} human EGF (Peprotech), 500nM A83-01 (Tocris), 10nM Gastrin (Tocris), 50% Wnt3a conditioned medium, 10mM Nicotinamide (Sigma), 10μM SB202190 (Sigma), 10nM Prostaglandin E2 (Tocris), and 10μM Y-27632 (Abmole). Medium was changed every two days and the expanding organoids were passaged by physical dissociation using fire-polished glass

Pasteur pipette every 6-7 days. To differentiate organoids, expanding SI organoids were grown in a Wnt-rich medium for 6-7 days after splitting and replaced with a differentiation medium (withdrawal Wnt, Nicotinamide, SB202190, Prostaglandin E2 from a Wnt-rich medium) and grown in a differentiation medium for 5 days 2.

Lung tissue was dissociated in lung organoid medium containing 1-2mg ml^{-1} collagenase (Sigma) at 37°C for 1-2 h. After washing and filtering with a a 100μm strainer, cell pellets were embedded in BME type 2 (Trevigen) and were cultured in lung organoid medium containing Advanced DMEM/F12 with 1x Glutamax, 10 mM HEPES, penicillin-streptomycin, 1x B27 (all from Invitrogen), 1μM *N*-Acetylcysteine (Sigma), 10% R-spondin1 conditioned medium, 10% Noggin conditioned medium, 25ng ml^{-1} human FGF7 (Peprotech), 100ng ml^{-1} human FGF10 (Peprotech), 500nM A83-01 (Tocris), 10mM Nicotinamide (Sigma), 1μM SB202190 (Sigma), and 10μM Y-27632 (Abmole). Medium was changed every 4 days and organoids were passaged every 2 weeks (Sachs et al., under revision).

Expanding SI organoids were microinjected at 5-6 days after seeding, differentiated SI organoids were injected at 5 days after inducing differentiation. Lung organoids were incubated for 2 weeks after seeding for microinjection.

For long-term culturing of the parasite, oocysts were injected in expanding organoids. The injected organoids were grown in expansion medium for 2-3 days and then 3-4 days in differentiated medium. At day 7, the organoids were split to 1:2. After splitting, organoids were grown in expansion medium for 2-3 days and then replaced with differentiated medium for 3-4 days until next split. The organoids were split every 7 days for 28 days.

Preparations of *Cryptosporidium parvum* (*C. parvum*) oocysts and sporozoites for microinjection

C. parvum oocysts (Iowa strain, The University of Arizona) were stored in sterile phosphate-buffered saline (PBS) with penicillin and streptomycin at 4°C and used within 2 months. For microinjection, about $1X10^7$ oocysts were incubated in 10% (v/v) Clorox bleach in PBS on ice and washed three times by centrifugation (for 3 min, at 8000 g, at 4 °C) with 1 ml DMEM. The oocysts were resuspended in 100μl organoid culture medium supplemented with 0.5% (w/v) sodium taurocholate (Sigma). To visualize injection, 0.05% (w/v) non-toxic FastGreen dye (Sigma) was also added to the suspension. The medium supplemented with the same amount of sodium taurocholate and FastGreen dye was used for control injection.

For sporozoite-microinjection, oocysts were pretreated with bleach and washed as described above. About 2 x 10^7 oocysts were incubated in 2-3 ml organoid culture medium supplemented with 0.75% (w/v) sodium taurocholate at 37°C for 60-90 min. Excystation efficiency was checked using microscopy (generally 50-60%). The sporozoites were filtered through a 3μM polycarbonate filter (Millipore) to remove unexcysted oocysts and oocyst shells, and washed by centrifugation (for 20 min, at 3400g, at 4°C) with cold DMEM. The sporozoites were resuspended in 50-100μl organoid culture medium supplemented with 0.05% (w/v) FastGreen dye, reducing agents (0.5μg/μl each glutathione, taurine, betaine, and cysteine) and 6.8μg/ml α-linolenic acid 20.

Microinjection

A glass capillary of 1mm diameter (WPI) was pulled by micropipette puller (Shutter Instrument) and the tip of the capillary was cut by sharp blade (the size of the capillary end is 9-12μm). Then, the capillary was filled with oocyst- or sporozoite- suspension by microloader tip (Eppendorf). The filled capillary was loaded in Femtojet 4i microinjector (Eppendorf) and used for microinjection. Around 100-200nl of suspension was injected into each organoid.

RNA isolation and quantitative RT-PCR (qRT-PCR)

Same number of oocysts were injected in the organoids in one drop of Matrigel. Total RNA was extracted from organoids in 1-2 drops of Matrigel using RNeasy Micro Kit (Qiagen) according to manufacturer's protocol including DNaseI treatment. To normalize, 1ng GFP messenger RNA was added to each sample during RNA extraction. cDNA was synthesized from 1μg of total RNA using GoScript and random primer (both Promega). qPCR was performed in triplicate using the indicated primers, IQ SYBR green (BioRad), and BioRad systems. Gene expression was quantified using the ΔΔCt method. Ct value of GFP was used for normalization. ΔCt of organoids at 0 day post-injection was used as control to calculate the ratio of 18S rRNA at each time point. Cp18S F, 5'-TTGTTCCTTACTCCTTCAGCAC-3'; Cp18S R, 5'-TCCTTCCTATGTCTGGACCTG-3' 43, 44.

Electron microscopy

For scanning electron microscopy, organoids were collected and incubated in Cell recovery solution (Corning) on ice for 20-30 min to remove Matrigel and fixed with 1% (v/v) glutaraldehyde (Sigma) in PBS at 4°C overnight and transferred onto 12mm poly-L-lysine coated coverslips (Corning). The organoids were serially dehydrated by consecutive 10min incubations in 2ml of 10% (v/v), 25% (v/v) and 50% (v/v) ethanol-PBS, 75% (v/v) and 90% (v/v) ethanol-H_2O, and 100% ethanol (2x), followed by 50% (v/v) ethanol-hexamethyldisilazane (HMDS) and 100% HMDS (Sigma). Coverslips were removed from the 100% HMDS and air-dried overnight at room temperature. Organoids were manipulated with 0.5mm tungsten needles using an Olympus SZX9 light microscope and mounted onto 12mm specimen stubs (Agar Scientific). Following gold-coating to 1nm using a Q150R sputter coater (Quorum Technologies) at 20mA, samples were examined with a Phenom PRO table-top scanning electron microscope (Phenom-World).

For transmission electron microscopy, organoids were placed in Matrigel on 3mm diameter and 200μm depth standard flat carriers for high pressure freezing and immediately cryoimmobilized using a Leica EM high-pressure freezer (equivalent to the HPM10), and stored in liquid nitrogen until further use. They were freeze-substituted in anhydrous acetone containing 2% osmium tetroxide and 0.1% uranyl acetate at –90 °C for 72 hr and warmed to room temperature, 5ºC per hour (EM AFS-2, Leica, Vienna, Austria). The samples were kept 2 hr at 4ºC and 2 hr more at room temperature. After several acetone rinses (4x15 min), samples were infiltrated with Epon resin for 2 days (acetone: resin 3:1- 3hr; 2:2 – 3hr; 3:1 – overnight; pure resin- 6hr + overnight + 6hr + overnight + 3hr). Resin was polymerised at 60ºC during 96 hr. Ultrathin sections from the resin blocks were obtained using a Leica

Ultracut UC6 ultramicrotome and mounted on Formvar-coated copper grids. They were stained with 2% uranyl acetate in water and lead citrate. Sections were observed in a Tecnai T12 Spirit equipped with an Eagle 4kx4k camera (FEI Company, The Netherlands) and large EM overviews were collected using the principles and software described previously45.

For transmission electron microscopy of isolated oocysts from the organoids, isolated oocysts were washed 3 times with PBS and fixed overnight at 4 degrees in ½ Karnovsky's Fixative (2% paraformaldehyde, 2.5% glutaraldehyde, in 0.1M Cacodylate buffer pH 7.2). The samples were then microwaved in a Pelco Biowave Pro 36500 Laboratory Microwave (Ted Pella Inc., Redding, CA. USA) for 45 sec at 200W with a temperature restriction of 35°C. The samples were rinsed with 0.1M Cacodylate buffer pH 7.2 and post fixed in a 2% buffered OsO4 for 2 hr at room temperature. The samples were rinsed with water and dehydrated with a 10% graded EtOH series. The samples were infiltrated overnight with one part propylene oxide and one part Spurr's resin. The cap was removed and the propylene oxide was allowed to evaporate overnight. The resin was exchanged 3X with fresh 100% Spurr's resin and left overnight. The samples were embedded in new Spurr's resin and cured for 24 hr at 70°C. Thin sections of approximately 70nm were taken with a Leica Reichert Ultracut R (Leica Microsystems, Wetzlar, Germany) equipped with a diamond knife and placed on formvar coated slot grids. The samples were stained for 20 min in 2% Uranyl acetate (aqueous) and for 6 min in Reynolds lead. Micrographs were taken with a FEI Technai G2 20 Twin TEM (Thermo Fisher Scientific, Waltham, MA. USA).

Immunofluorescence staining

Organoids were collected and incubated in Cell recovery solution (Corning) on ice for 20-30 min to remove Matrigel. The organoids were fixed with 4% paraformaldehyde overnight at 4°C, permeabilized with 0.2% v/v Triton X-100 (Sigma) in PBS at room temperature for 20 min, and incubated in blocking solution (2% v/v goat serum, 0.1% v/v Tween-20 in PBS) at room temperature for 1 hr. The organoids were subsequently incubated with anti-gp15 antibody diluted in blocking solution at 4 °C overnight, washed three times with 0.1% Tween-20 in PBS and incubated with secondary antibody (Alexa 568 goat anti-rabbit), phalloidin-Alexa 674, and DAPI (all Invitrogen) at room temperature for 2hr. After three times of washing with 0.1% Tween-20 PBS, a fluorescein-labeled antibody Crypt-a-Glo® or Sporo-Glo® (Waterborne) was added to label oocysts or intracellular stages of the parasite, respectively, and incubated at room temperature for 1 hr. After washing once with 0.1% Tween-20 PBS, the organoids were mounted in VECTASHIELD hard-set antifade mounting medium (VectorLabs). Samples were imaged on SP8 confocal microscopes using LAS X software (all Leica) and processed using ImageJ.

Isolation of oocysts from organoids

Organoids were collected, incubated in Cell recovery solution (Corning) on ice for 20-30 min to remove Matrigel and washed twice with cold DMEM. The organoids were suspended in water, physically dissociated by pipetting and homogenization, and combined with magnetic beads coated in monoclonal antibody reactive with the *Cryptosporidium* oocyst surface (Crypto-Grab IMS beads, Waterborne, Inc, New Orleans, LA). Oocysts were isolated by immunomagnetic separation and eluted off the beads following manufacturer's

Europe PMC Funders Author Manuscripts

recommendations. Isolated oocysts were dried onto Superstick slides (Waterborne), fixed in methanol and reacted with a fluorescein-labeled monoclonal antibody to the *Cryptosporidium* oocyst wall (Crypt-a-Clo®, Waterborne). Slides were mounted in VECTASHIELD, and visualized on a Leica SP8 Point Scanning Confocal Microscope.

Animal experiments

Mouse experiments consisted of 4 mice (both genders used) per group. Due to the young age (8 day olds) and traumatic nature of defining sex in the neonatal mice, gender was not determined. Groups were 1) control uninjected organoids 2) infected organoids 3) commercially available oocysts (Iowa strain, obtained from calves, University of Arizona) as a positive control. The sample size was chosen to generate statistically significant data on the infectious nature of the newly generated oocysts in organoids and compare the infection rate to commercially available oocysts. Sample size was based on the expected variation within groups, the expected differences between groups, and the probable degrees of freedom necessary to detect significant differences and validate conclusions. For this evaluation, one tailed Student's t test and one-way ANOVA was used to compare mean infection scores between test and control groups. The assignment of animals within the three groups was done randomly using Microsoft Excel Random Number Generation Tool. All mice used in the present study were maintained in Biosafety Level 2 (BSL-2) biocontainment at the University of Arizona in accordance with the PHS Guide for the Care and Use of Laboratory Animals and IACUC approval.

Mouse Infection experiments

At 24 hr or 96-120 hr after sporozoite- or control media- infection, differentiated SI organoids were collected and incubated in Cell recovery solution (Corning) on ice for 20-30 min to remove Matrigel. The organoids were washed twice with 10ml cold DMEM. The organoids were physically dissociated by pipetting several times with fire-polished glass Pasteur pipette and centrifuged for 20 min at 4000rpm at 4°C. The pellet was resuspended in saline for inoculation.

Ten specific-pathogen-free (SPF) ICR mice were used in the study. Mice were administered with 100μl broken organoids (four mice per each sporozoite-injected organoids or control organoids) or 1X10e4 *C. parvum* oocysts (Iowa strain, for two mice) by gastric intubation. After euthanasia at 92 to 94 hr post-infection, longitudinal sections representing the entire length of the jejunum, ileum, cecum, and colon were collected, processed for histopathology and stained with hematoxylin and eosin. Slides were then examined histologically for *C. parvum* stages in mucosal epithelium46.

To quantify the level of infection with *C. parvum*, qPCR was performed as described previously31. The entire intestine was extracted from each mouse and homogenized using ceramic beads in the Bead Ruptor4 (OMNI International, Kennesaw, GA). DNA was extracted using the QIAamp Fast DNA stool mini kit (Qiagen, Gaithersburg, MD) with the following modifications. After the addition of InhibitEx buffer, the samples were incubated at 95°C for 5 min, followed by 5 freeze-thaw cycles using liquid nitrogen and a 37°C water bath. Total DNA in the samples was quantified by Nanodrop (Thermo Scientific, Waltham,

MA). The *C. parvum* heat shock protein gene (HSP70) was chosen as the target for primers (CpHSP70F, 5'- AACTTTAGCTCCAGTTGAGAAAGTACTC-3'; CpHSP70R, 5'-CATGGCTCTTTACCGTTAAAGAATTCC-3', and TaqMan probe CpHSP70 5'-AATACGTGTAGAACCACCAACCAATACAACATC-3'). The Taqman probe was labelled at the 5'-end with the 6-carboxyfluorescein reporter dye (FAM) and at the 3'-end with the 6-carboxytetramethylrhodamine quencher dye (TAMRA). For qPCR, each 20μl reaction contained a final concentration of 300nM for forward primer, 900nM for reverse primer (Invitrogen, Grand Island, NY), and 200nM for Taqman probe (Applied Biosystems, Foster City, CA), 10μl Mastermix (Applied Biosystems). Genomic DNA (2μl) was added and the PCR was performed in an ABI StepOne Plus Real-Time PCR System (Applied Biosystems, Grand Island, NY) with cycling conditions of 15 min incubation at 95°C followed by 40 cycles at 94°C for 15sec and 60°C for 1 min. Each sample was run in triplicate. A control with no template was run concurrently and was consistently negative. For standards, 1X10e6, 5X10e5, 1X10e5, 5X10e4, 1X10e4, 5X10e3, and 1X10e3 oocysts were used to extract genomic DNA and do qPCR with the same protocol described above. Standard curve was generated using StepOne Plus real-time PCR machine software. Numbers of *C. parvum* stages were calculated by comparison to this standard curve.

RNA sequencing

Organoids derived from two independent donors were microinjected with oocyst or control media. Total RNA was extracted from collected organoids at 24 and 72 hr post-injection using RNeasy Micro Kit (Qiagen) according to manufacturer's protocol including DNaseI treatment. Quality and quantity of isolated RNA was checked and measured with Bioanalyzer 2100 RNA Nano 6000 chips (Agilent). Libraries were prepared as described previously47 and sequenced on an Illumina NextSeq500 by using 75-bp paired-end sequencing. Paired-end reads from Illumina sequencing were aligned to the human transcriptome genome and *C. parvum* transcriptome genome (Iowa strain) by BWA48. DeSeq (v1.18.0) was used for read normalization and differential expression analysis. Gene set enrichment analysis (GSEA) was performed using gene lists for type I interferon response and regulation against normalized RNA-seq reads of injected SI and lung organoids using GSEA software v3.0 beta2.

GO-term analysis of *C. parvum* genes

Categories were assigned to the 216 significantly (p-value <0.05) and differentially expressed genes of lung and SI organoids at 24 or 72 hr post-injection by leveraging data available on CryptoDB (http://cryptodb.org)49. First, initial categories were prepared using computed gene ontology (GO) biologic processes. Umbrella biologic processes categories were chosen for computed processes that were very specific (e.g., GO:0006810, transport instead of GO:0006605, protein targeting) using the inferred tree view of AmiGO 2 (http://amigo.geneontology.org). Next, uncategorized genes were grouped into existing umbrella categories using computed GO functions using the same method as before. The remaining uncategorized genes were categorized by protein product description provided by curators of CryptoDB (e.g., hypothetical protein, oocyst wall proteins, mucins, ribosomal proteins, secreted, etc.). Data analysis and visualization of the number and percent of highly expressed genes in each category for each condition was accomplished in R.

Supplementary Material

Refer to Web version on PubMed Central for supplementary material.

Acknowledgments

We are grateful to Anna Alemany Arias, Jens Puschhof and Huili Hu for assistance with mapping of RNA sequencing data, the Franceschi Microscopy and Imaging Center and Daniel L. Mullendore at Washington State University for TEM preparation and imaging of isolated organoid oocysts, and Chirlmin Joo, Joep Beumer and Oded Kopper for discussions and critical reading of the manuscript. I.H. is the recipient of a VENI grant from the Netherlands Organization for Scientific Research (NWO-ALW, 863.14.002) and was supported by Marie Curie fellowships from the European Commission (Proposal 330571 FP7-PEOPLE-2012-IIF). D.D. is the recipient of a VENI grant from the Netherlands Organization for Scientific Research (NWO-ALW, 016.Veni.171.015). The research leading to these results has received funding from the European Research Council under ERC Advanced Grant Agreement n. 67013 and from NIH NIAIH under R21 AT009174. This work is part of the Oncode Institute which is partly financed by the Dutch Cancer Society and was funded by a grant from the Dutch Cancer Society.

References

1. Clevers H. Modeling Development and Disease with Organoids. Cell. 2016; 165:1586–1597. [PubMed: 27315476]
2. Sato T, et al. Long-term expansion of epithelial organoids from human colon, adenoma, adenocarcinoma, and Barrett's epithelium. Gastroenterology. 2011; 141:1762–1772. [PubMed: 21889923]
3. Bouzid M, Hunter PR, Chalmers RM, Tyler KM. Cryptosporidium pathogenicity and virulence. Clinical microbiology reviews. 2013; 26:115–134. [PubMed: 23297262]
4. Thompson RC, et al. Cryptosporidium and cryptosporidiosis. Advances in parasitology. 2005; 59:77–158. [PubMed: 16182865]
5. Current WL, Garcia LS. Cryptosporidiosis. Clinics in laboratory medicine. 1991; 11:873–897. [PubMed: 1802526]
6. Hunter PR, Nichols G. Epidemiology and clinical features of Cryptosporidium infection in immunocompromised patients. Clinical microbiology reviews. 2002; 15:145–154. [PubMed: 11781272]
7. Checkley W, et al. A review of the global burden, novel diagnostics, therapeutics, and vaccine targets for cryptosporidium. The Lancet Infectious diseases. 2015; 15:85–94. [PubMed: 25278220]
8. Liu L, et al. Global, regional, and national causes of child mortality: an updated systematic analysis for 2010 with time trends since 2000. Lancet. 2012; 379:2151–2161. [PubMed: 22579125]
9. Sponseller JK, Griffiths JK, Tzipori S. The evolution of respiratory Cryptosporidiosis: evidence for transmission by inhalation. Clinical microbiology reviews. 2014; 27:575–586. [PubMed: 24982322]
10. Mor SM, et al. Expectoration of Cryptosporidium Parasites in Sputum of Human Immunodeficiency Virus-Positive and -Negative Adults. The American journal of tropical medicine and hygiene. 2018
11. Kotloff KL, et al. Burden and aetiology of diarrhoeal disease in infants and young children in developing countries (the Global Enteric Multicenter Study, GEMS): a prospective, case-control study. Lancet. 2013; 382:209–222. [PubMed: 23680352]
12. Amadi B, et al. Effect of nitazoxanide on morbidity and mortality in Zambian children with cryptosporidiosis: a randomised controlled trial. Lancet. 2002; 360:1375–1380. [PubMed: 12423984]
13. Amadi B, et al. Reduced production of sulfated glycosaminoglycans occurs in Zambian children with kwashiorkor but not marasmus. The American journal of clinical nutrition. 2009; 89:592–600. [PubMed: 19116330]
14. Striepen B. Parasitic infections: Time to tackle cryptosporidiosis. Nature. 2013; 503:189–191. [PubMed: 24236315]
15. Lendner M, Daugschies A. Cryptosporidium infections: molecular advances. Parasitology. 2014; 141:1511–1532. [PubMed: 24679517]

16. Karanis P, Aldeyarbi HM. Evolution of Cryptosporidium in vitro culture. International journal for parasitology. 2011; 41:1231–1242. [PubMed: 21889507]
17. Karanis P. The truth about in vitro culture of Cryptosporidium species. Parasitology. 2017:1–10.
18. Varughese EA, Bennett-Stamper CL, Wymer LJ, Yadav JS. A new in vitro model using small intestinal epithelial cells to enhance infection of Cryptosporidium parvum. Journal of microbiological methods. 2014; 106:47–54. [PubMed: 25072838]
19. Castellanos-Gonzalez A, Cabada MM, Nichols J, Gomez G, White AC Jr. Human primary intestinal epithelial cells as an improved in vitro model for Cryptosporidium parvum infection. Infection and immunity. 2013; 81:1996–2001. [PubMed: 23509153]
20. Morada M, et al. Continuous culture of Cryptosporidium parvum using hollow fiber technology. International journal for parasitology. 2016; 46:21–29. [PubMed: 26341006]
21. DeCicco RePass MA, et al. Novel Bioengineered Three-Dimensional Human Intestinal Model for Long-Term Infection of Cryptosporidium parvum. Infection and immunity. 2017; 85
22. Dutta D, Heo I, Clevers H. Disease Modeling in Stem Cell-Derived 3D Organoid Systems. Trends in molecular medicine. 2017; 23:393–410. [PubMed: 28341301]
23. McCracken KW, et al. Modelling human development and disease in pluripotent stem-cell-derived gastric organoids. Nature. 2014; 516:400–404. [PubMed: 25363776]
24. Ettayebi K, et al. Replication of human noroviruses in stem cell-derived human enteroids. Science. 2016; 353:1387–1393. [PubMed: 27562956]
25. Umemiya R, Fukuda M, Fujisaki K, Matsui T. Electron microscopic observation of the invasion process of Cryptosporidium parvum in severe combined immunodeficiency mice. The Journal of parasitology. 2005; 91:1034–1039. [PubMed: 16419745]
26. Aldeyarbi HM, Karanis P. The fine structure of sexual stage development and sporogony of Cryptosporidium parvum in cell-free culture. Parasitology. 2016; 143:749–761. [PubMed: 26935529]
27. Aldeyarbi HM, Karanis P. Electron microscopic observation of the early stages of Cryptosporidium parvum asexual multiplication and development in in vitro axenic culture. European journal of protistology. 2016; 52:36–44. [PubMed: 26587578]
28. Aldeyarbi HM, Karanis P. The Ultra-Structural Similarities between Cryptosporidium parvum and the Gregarines. The Journal of eukaryotic microbiology. 2016; 63:79–85. [PubMed: 26173708]
29. Fayer, R., Xiao, L. Cryptosporidium and cryptosporidiosis. 2nd Edition. 2008.
30. Ernest JA, Blagburn BL, Lindsay DS, Current WL. Infection dynamics of Cryptosporidium parvum (Apicomplexa: Cryptosporiidae) in neonatal mice (Mus musculus). The Journal of parasitology. 1986; 72:796–798. [PubMed: 3806334]
31. Shahiduzzaman M, Dyachenko V, Obwaller A, Unglaube S, Daugschies A. Combination of cell culture and quantitative PCR for screening of drugs against Cryptosporidium parvum. Veterinary parasitology. 2009; 162:271–277. [PubMed: 19342176]
32. Riggs MW, Perryman LE. Infectivity and neutralization of Cryptosporidium parvum sporozoites. Infection and immunity. 1987; 55:2081–2087. [PubMed: 3623693]
33. Sachs N, et al. Long-term expanding human airway organoids for disease modelling. BioRxiv. 2018; doi: 10.1101/318444
34. Beiting DP. Protozoan parasites and type I interferons: a cold case reopened. Trends in parasitology. 2014; 30:491–498. [PubMed: 25153940]
35. Barakat FM, McDonald V, Foster GR, Tovey MG, Korbel DS. Cryptosporidium parvum infection rapidly induces a protective innate immune response involving type I interferon. The Journal of infectious diseases. 2009; 200:1548–1555. [PubMed: 19821721]
36. Frenal K, Soldati-Favre D. Role of the parasite and host cytoskeleton in apicomplexa parasitism. Cell host & microbe. 2009; 5:602–611. [PubMed: 19527887]
37. Elliott DA, et al. Cryptosporidium parvum infection requires host cell actin polymerization. Infection and immunity. 2001; 69:5940–5942. [PubMed: 11500478]
38. Rayamajhi M, Humann J, Penheiter K, Andreasen K, Lenz LL. Induction of IFN-alphabeta enables Listeria monocytogenes to suppress macrophage activation by IFN-gamma. The Journal of experimental medicine. 2010; 207:327–337. [PubMed: 20123961]

39. O'Connell RM, et al. Type I interferon production enhances susceptibility to Listeria monocytogenes infection. The Journal of experimental medicine. 2004; 200:437–445. [PubMed: 15302901]
40. In J, et al. Enterohemorrhagic Escherichia coli reduce mucus and intermicrovillar bridges in human stem cell-derived colonoids. Cellular and molecular gastroenterology and hepatology. 2016; 2:48–62 e43. [PubMed: 26855967]
41. Vinayak S, et al. Genetic modification of the diarrhoeal pathogen Cryptosporidium parvum. Nature. 2015; 523:477–480. [PubMed: 26176919]
42. Blokzijl F, et al. Tissue-specific mutation accumulation in human adult stem cells during life. Nature. 2016; 538:260–264. [PubMed: 27698416]
43. Zhou R, Gong AY, Eischeid AN, Chen XM. miR-27b targets KSRP to coordinate TLR4-mediated epithelial defense against Cryptosporidium parvum infection. PLoS pathogens. 2012; 8:e1002702. [PubMed: 22615562]
44. Chen XM, Splinter PL, O'Hara SP, LaRusso NF. A cellular micro-RNA, let-7i, regulates Toll-like receptor 4 expression and contributes to cholangiocyte immune responses against Cryptosporidium parvum infection. The Journal of biological chemistry. 2007; 282:28929–28938. [PubMed: 17660297]
45. Faas FG, et al. Virtual nanoscopy: generation of ultra-large high resolution electron microscopy maps. The Journal of cell biology. 2012; 198:457–469. [PubMed: 22869601]
46. Riggs MW, et al. Protective monoclonal antibody defines a circumsporozoite-like glycoprotein exoantigen of Cryptosporidium parvum sporozoites and merozoites. Journal of immunology. 1997; 158:1787–1795.
47. Grun D, et al. Single-cell messenger RNA sequencing reveals rare intestinal cell types. Nature. 2015; 525:251–255. [PubMed: 26287467]
48. Li H, Durbin R. Fast and accurate short read alignment with Burrows-Wheeler transform. Bioinformatics. 2009; 25:1754–1760. [PubMed: 19451168]
49. Heiges M, et al. CryptoDB: a Cryptosporidium bioinformatics resource update. Nucleic acids research. 2006; 34:D419–422. [PubMed: 16381902]

Europe PMC Funders Author Manuscripts

Europe PMC Funders Author Manuscripts

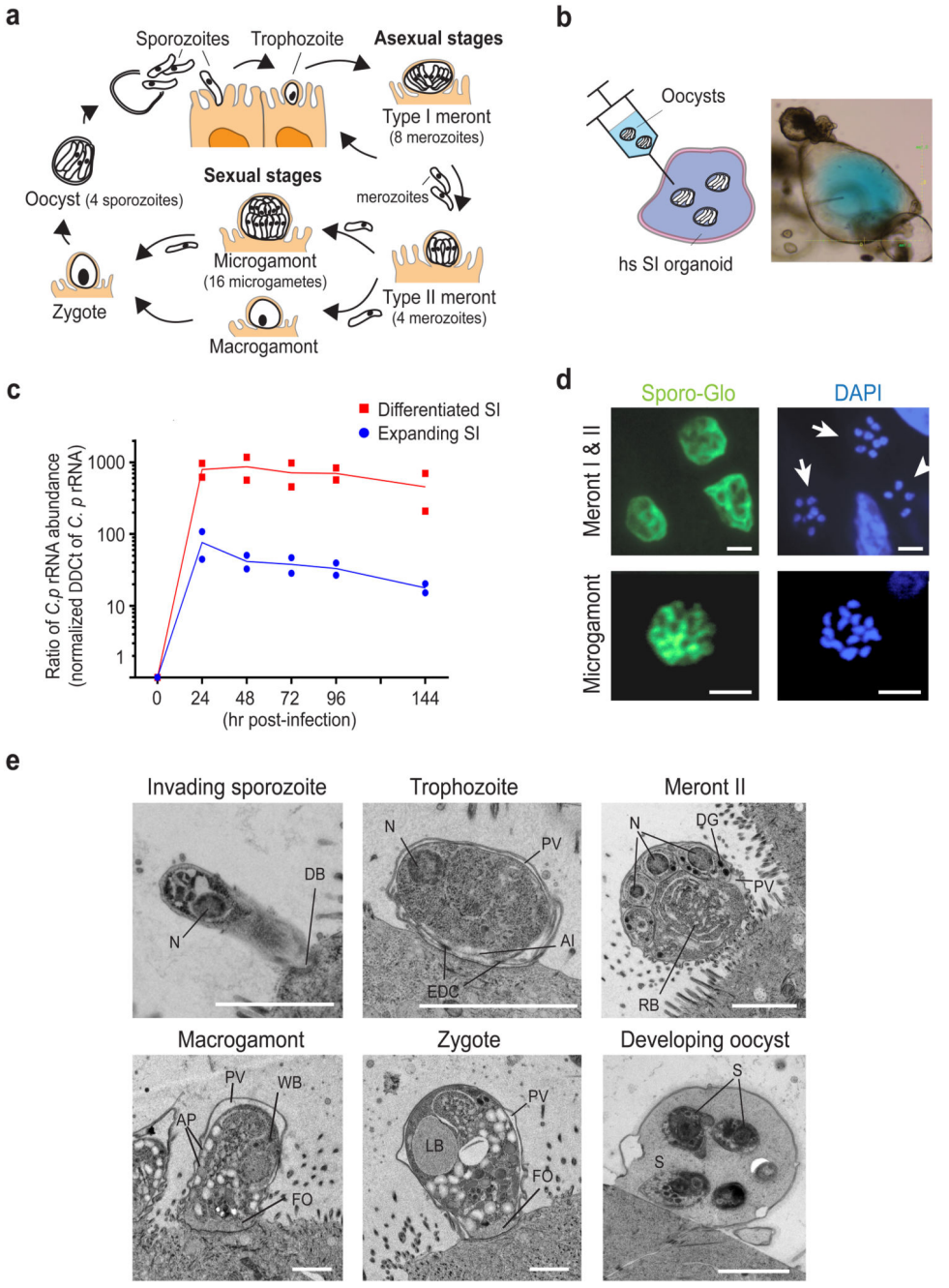

Figure 1. Development of asexual and sexual stages of *C. parvum* in human SI organoids.

(a) Schematic representation of *C. parvum* life cycle.

(b) Scheme and bright-field images of microinjection.

(c) *C. parvum* 18S rRNA was measured at each time point after injection in differentiated and expanding SI organoids by qRT-PCR (n=2 biologically independent experiments). Mean value at each time point was used for connecting line.

(d) Immunofluorescence of *C. parvum* epicellular stages in expanding organoids. (top) At 24 hr post-injection, meront I (arrow) and possibly meront II (arrowhead) were observed.

(bottom) At 72 hr, a microgamont with 16 nuclei was detected. Sporo-Glo marks epicellular stages. DAPI mark nuclei. Scale bars indicate 2μm. More than 40 meronts I, 10 meronts II and 3 microgamonts were observed independently.

(e) TEM of distinct stages of *C. parvum* life cycle after injection. Invading sporozoite and meront II were observed in differentiated organoids at 1 day. Trophozoite was observed in expanding organoid at 1 day. PV: parasitophorous vacuole, FO: feeder organelle, AP: amylopectin granule, WB: wall-forming body, LB: lipid body, DG: dense granule, N: nucleus, RB: residual bod, DB: dense band, EDC: electron dense collar, AI: anterior invagination. Scale bars indicate 2μm. Macrogamont, zygote and developing oocyst were detected in expanding organoids at 5 day. More than 2 sporozoites, 4 trophozoites, 5 meronts II, 5 macrogamonts, 1 zygote and 3 oocysts were observed independently.

Europe PMC Funders Author Manuscripts

Europe PMC Funders Author Manuscripts

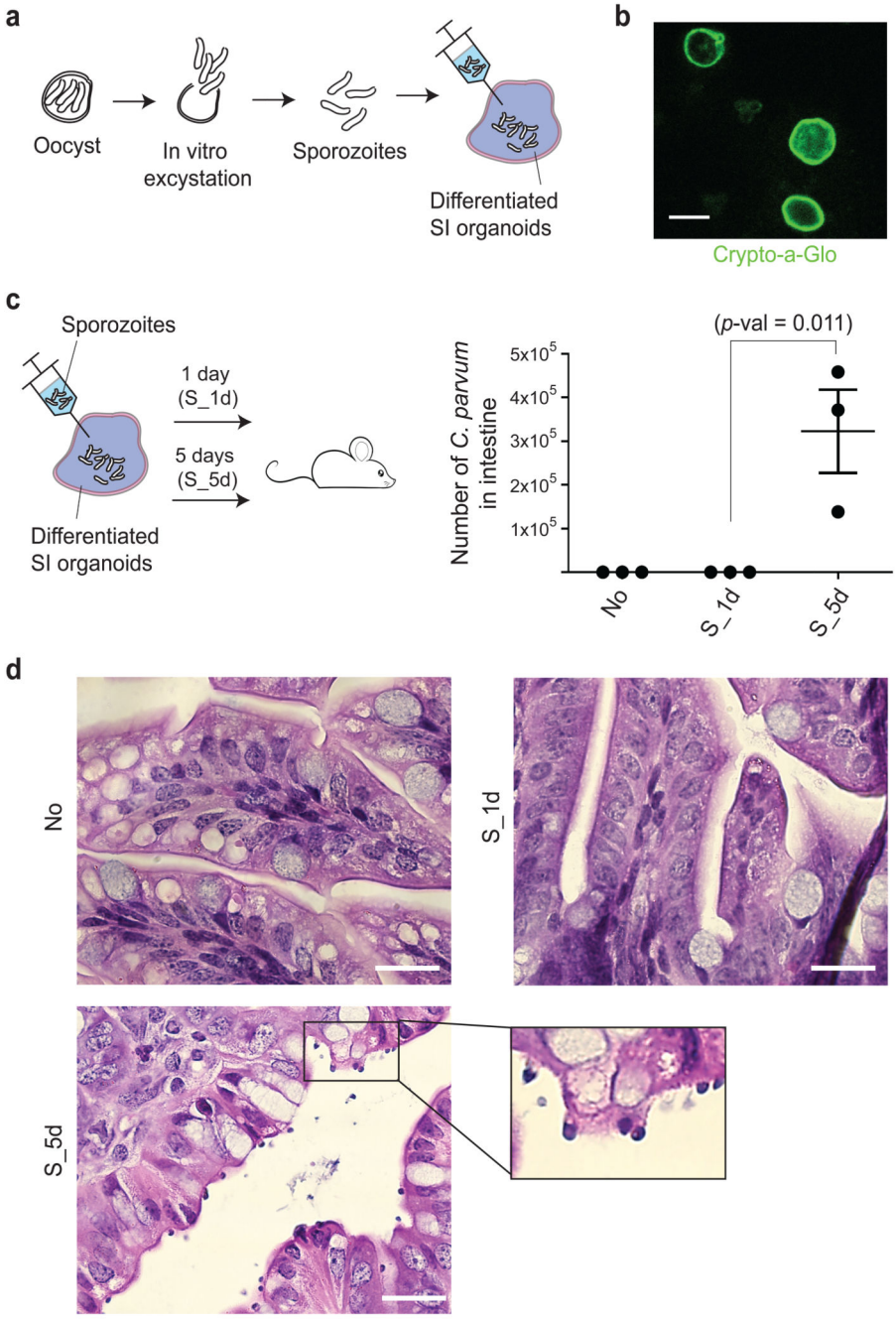

Figure 2. *C. parvum* completes its life cycle inside organoids.

(a) Schematic representation showing microinjection of *in vitro* excysting sporozoites.

(b) Immunofluorescence of *C. parvum* oocysts isolated from sporozoite-injected organoids at 4 day post-injection. Scale bars indicate 5μm. Isolated oocysts were observed from two independent experiments.

(c) (left) Schematic representation showing inoculation of sporozoite-injected organoids into neonatal mice (right). Scatter dot plot showing the level of infection in mice by sporozoite-injected organoids. At 94 hr post-inoculation of organoids, the level of *C. parvum* HSP70

gene in mice intestine was measure by qPCR (n=biologically 3 independent mice). Numbers of *C. parvum* stages were calculated by comparison to standards of known quantities of *C. parvum*. Organoids that were infected with sporozoites and incubated for 5 days (S_5d) were infectious to mice whereas organoids that were infected and incubated for 1 day (S_1d) were not (one-way ANOVA). The lines in the scatter dot plot depict the medians with error bars (± standard deviation).

(d) Histological section of the ileum-cecum junction of the inoculated mice. Scale bars indicate 1mm. Similar results were observed from two independent experiments.

Europe PMC Funders Author Manuscripts

Europe PMC Funders Author Manuscripts

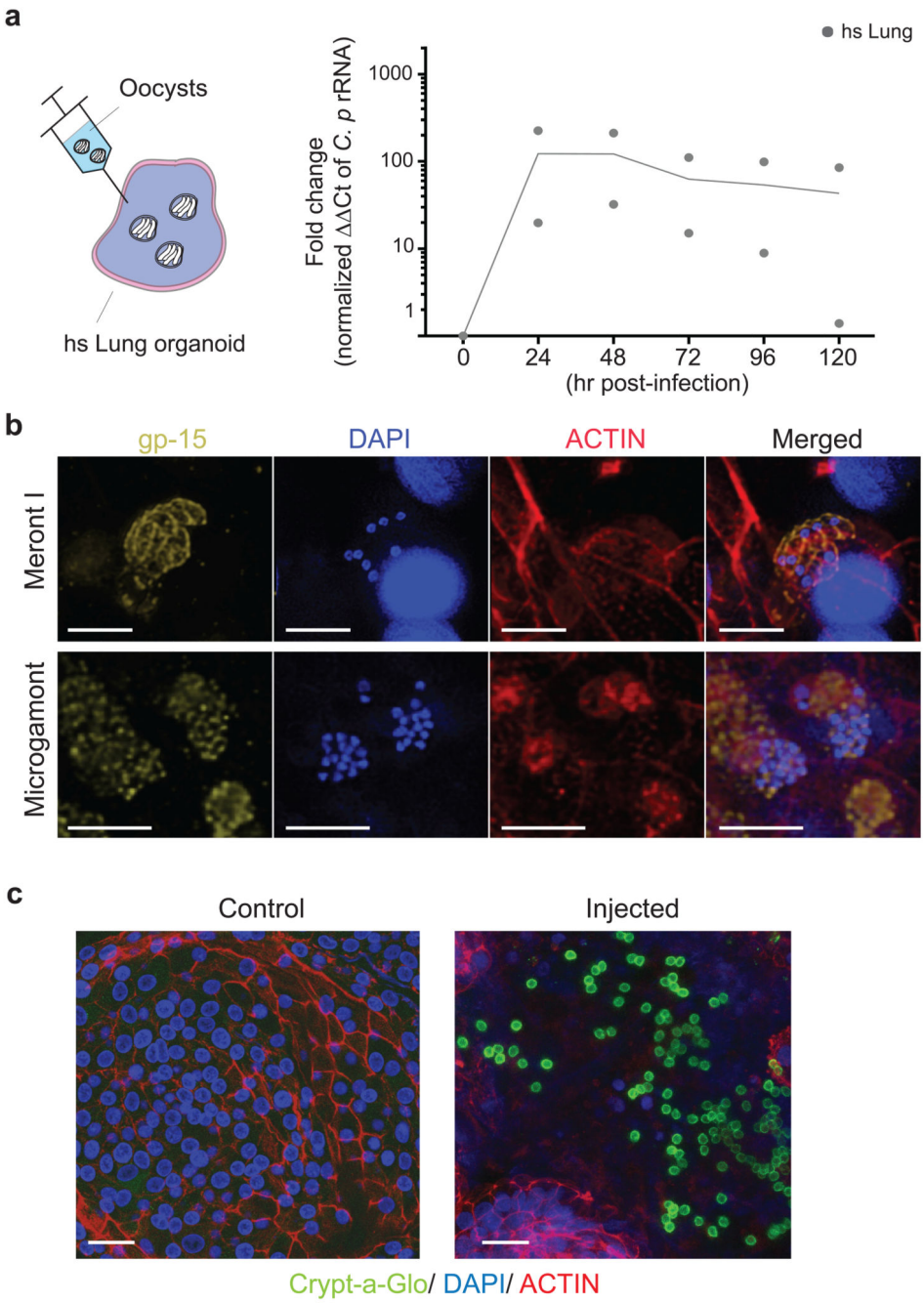

Figure 3. *In vitro* culture of *C. parvum* in human lung organoids

(a) (left) Schematic representation showing microinjection. (right) *C. parvum* 18S rRNA was measured at each time point after injection in lung organoids by qRT-PCR (n=2 biologically independent samples). Mean value at each time point was used for connecting line.

(b) Immunofluorescence of meront I and microgamont stages in lung organoids. Anti-gp-15 antibody (yellow) marks both merozoites in meront and microgametes in microgamont. Scale bars indicate 5μm. More than 20 meronts I and 5 microgamonts were observed.

(c) Immunofluorescence of newly formed oocysts inside lung organoids at 168 hr post-injection. Scale bars indicate 20μm. The oocysts were observed from more than 6 independent organoids. Media-injected organoids were used as a control.

Europe PMC Funders Author Manuscripts

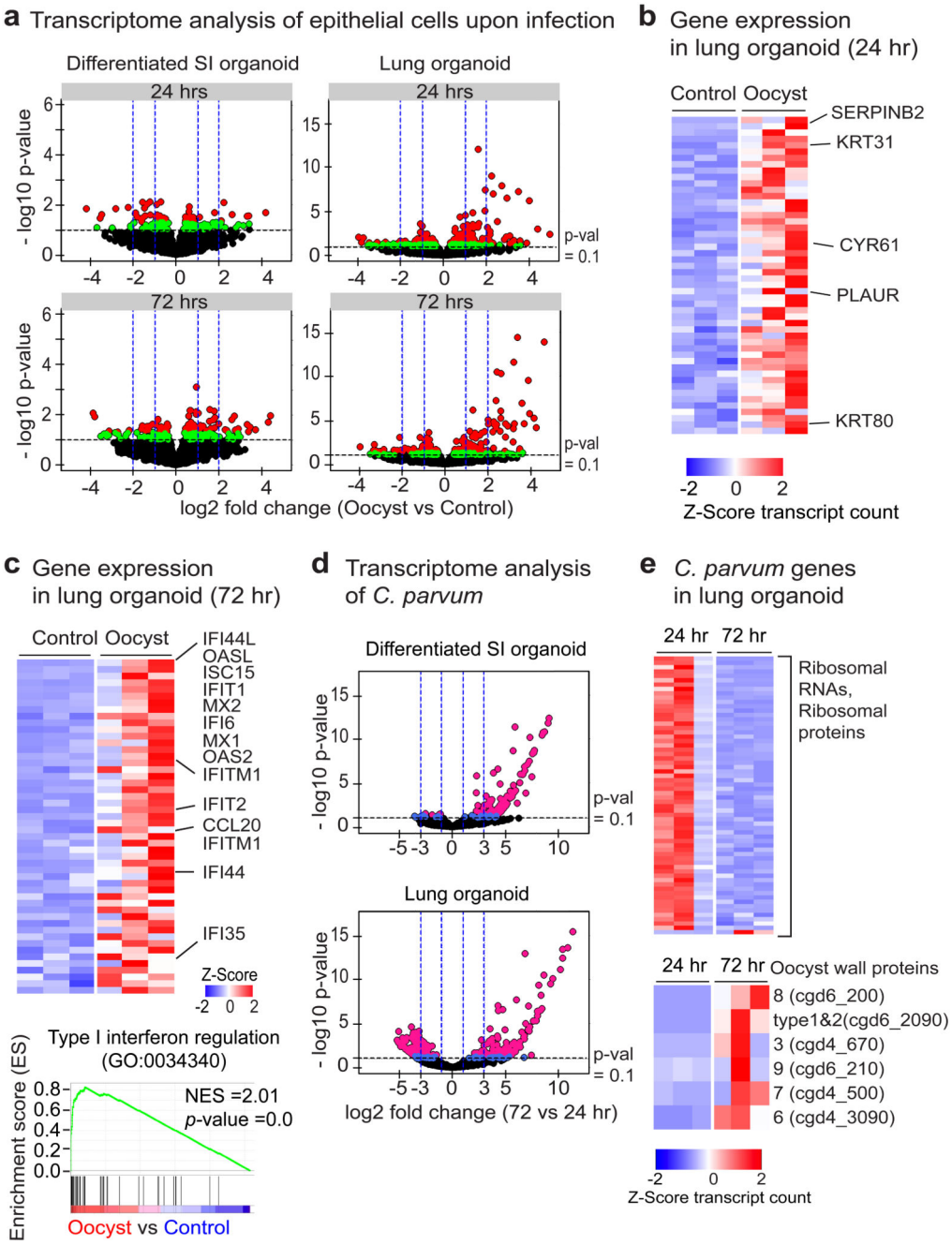

Figure 4. Transcriptome analysis of host epithelia and *C. parvum*.

(a) Volcano plot showing differential expression of host genes between oocyst- and media (control)-injected organoids at 24 and 72 hr post-injection (n=3 biologically independent samples). Each dot represents a gene. The red and green dots represent differentially expressed genes with *p*-value < 0.05 and with *p*-value <0.1 (Wald test), respectively upon injection. The vertical lines represent log2 fold change values as indicated in x axis. List of differentially expressed genes are available in Supplementary Table 1.

(b) Heatmap showing the expression of top 30 induced genes in lung organoids at 24 hr post-injection (n=3 biologically independent samples). Expression values are expressed as Z-score transformed transcript count.

(c) (top) Heatmap showing the expression of 30 induced genes in lung organoids at 72 hr post-inject (n=3 biologically independent samples). (bottom) Gene set enrichment assay (GSEA) plot showing strong enrichment of type I interferon regulation genes in oocyst-injected lung organoids. NES: normalized enrichment score, *p*-value is nominal *p*-value. Black bars underneath the graph present the rank position of genes from the gene set. GSEA plots of genes in differentiated SI organoids are available in Supplementary Fig. 5.

(d) Volcano plot showing differential expression of *C. parvum* genes between 24 and 72 hr post-injection into differentiated SI and lung organoids (n=3 biologically independent samples). The magenta and blue dots indicate enriched genes with p-value <0.05 and with p-value <0.1 (Wald test), respectively. List and GO-term analysis of differentially expressed *C. parvum* genes are available in Supplementary Table 2 and Fig 6, respectively.

(e) Heatmap showing the expression of ribosomal protein coding genes (top) and oocyst wall protein genes (bottom) of *C. parvum* in lung organoids at 24 and 72 hr post-injection (n=3 biologically independent samples). Heatmap of *C. parvum* genes in SI organoids are available in Supplementary Fig. 7.

Europe PMC Funders Author Manuscripts